IDENTIFICATION AND RISK MODELING OF AIRFIELD OBSTRUCTIONS FOR AVIATION SAFETY MANAGEMENT

Chun Wang, Yong Hu, Vincent Tao

GeoICT Lab, York University, 4700 Keele Street, Toronto M3J 1P3 - (chunwang, yhu, tao)@yorku.ca

KEY WORDS: Lidar, Obstruction Identification Surface, Identification, Risk Model, Impact Analysis

ABSTRACT:

The air safety is critical to the national security and economy. The aeronautical community has recognized the need for accurate 3-D geospatial information in and around the airfield to identify obstructions, specifically for accurate runway positions, obstruction locations and heights, and topography around airfields. In this paper, we present an approach to identify the airfield obstructions and model the risks by using advanced airborne lidar processing techniques. Airfield objects required for the analysis of the obstruction identification surface (OIS) are digitized from the aerial imagery and the topographic map, and their heights are derived using lidar data and the lidar-derived DTM. The 3-D OISs are created for runways to identify airfield obstructions based on the latest safety specification. A risk modeling approach is developed to classify the obstructions into three risk levels by combining four risk factors in a multi-criteria evaluation to assist decision-making in managing the airfield obstructions. The result is a risk-rating map that illustrates the high-, median-, and low-risk obstructions in 3-D. The presented approach is of important value to the examine whether their airfields meet the new safety specification.

1. INTRODUCTION

On April 3rd, 1996, Secretary of Commerce Ron Brown, 32 business executives, and US military personnel were killed in a plane crash in Dubrovnik, Croatia. This crash led US congress passed the Ron Brown Initiative in 2000 to survey glide slope obstructions on the approaches to some 7200 airports in the United States and an undetermined number of airports, worldwide. For a distance of 14km on each end of each runway, and for a specified distance around the entire airport complex, the geolocation and surveyed heights of all objects (building, trees, light poles, antennas and towers, power lines, and other physical features) must be recorded (Morain, 2001).

The aeronautical community has recognized the acute need for accurate 3-D geospatial information in and around the airfield critical to flight safety, specifically for accurate runway positions, obstruction locations and heights, and topography around airfields. Knowing the location of an aircraft is only half of the solution. To bring an aircraft safely onto the runway with little else than satellite navigation, the pilot will need very accurate and reliable geodetic coordinates for the landing runway. Currently, pilots are still expected to use conventional navigation aids or visual contact to direct the aircraft to the runway.

Airborne lidar is suitable for collecting accurate terrain data and providing feature information for airport safety management. In addition to identifying obstructions and designing approach procedures, pilots will be able to use the generated 3-D airfield models for flight training, pre-flight flythrough familiarizations, as well as increasing overall aircrew situational awareness relating to mission planning. The airfield initiative document (AID) is a newly published specification for airfield obstruction identification (NIMA, 2001). It describes the use of 3-D OISs to survey glide slope obstructions, and puts new requirements for a safer flying environment. "The OIS consists of several surfaces with certain dimensions related to a specific runway approach, including primary surface (PS), approach surface (AS), primary/approach

transitional surface (P/ATS), inner horizontal surface (IHA), conical surface (CS), outer horizontal surface (OHS), and conical/outer horizontal approach transition surface (C/OHATS)" (NIMA, 2001). When approaches share the exact surface, only one OIS is required. An obstruction is any object that penetrates an OIS, except where no obstruction penetrates the OIS; it shall be the highest object within the area. The obstructions are often extracted from photogrammetric and survey data. In addition, to avoid airport incursion, the surface of vehicular traverse ways (SVTW) is also needed (NIMA, 2001).

"The geospatial data required for obstruction identification around an airfield include the airfield elevation model (AEM), airfield features, and different combinations of the highest, the most penetrating, the highest approach and the highest non man-made obstructions/objects for analyzing each type of OIS surface" (NIMA, 2001). The AEM is in one arc second spacing each post having an absolute vertical accuracy of ±30.0 meters with respect to reflective surface. This vertical accuracy is required throughout the entire project area except for those posts that fall within the primary, primary approach and primary/approach transitional surfaces (NIMA, 2001). Airfield features, such as runway ends, must be surveyed to achieve high accuracy, for example, 0.3 m CE90 (circular error) and 0.07 m LE90 (linear error) for runway points. The required accuracy within OIS is lower. For example, within the PS, it is 6 m CE90 horizontally and 1 m LE90 vertically for the highest obstruction and the highest non man-made obstruction/object in each 912-m section of the primary area on each side of the runway. The required accuracies for other surfaces are normally lower.

2. STUDY AREA AND DATA DESCRIPTION

The study airport, Santa Barbara Airport, was selected by US Department of Transportation and Airfield Initiative Remote Sensing Technologies Evaluation Project as initiated case study followed by several site selection criteria (TRB, 2002):

1. Small to moderately sized airfield
2. Proximity to partners
3. Obstructions
4. Interest from airport administration

The city – Santa Barbara situated in a coastal valley between the Santa Ynez Mountains and the Pacific Ocean. The airport is located on west of the city. Santa Barbara airport has three runways (see Figure 1). One is in east-west direction; another two are in the direction from southeast to northwest. At the north part, there are hills with varying heights. There are only a few large buildings around the airport, and most residential buildings are both smaller and lower than forested clusters. The airfield features are surveyed in field, including runway polygon and end points, taxiway, touchdown zone, overrun stop way, apron hardstand, buildings, roads, inland water areas, airfield elevation points, and many obstructions. The lidar dataset covers only the areas within the IHS. It consists of 11.3 million first-return lidar points covering an area of 26 km^2. The terrain relief is from 0.31 m to 148.51 m. An aerial color digital orthorectified quadrangle (DOQ) with a 1-m GSD covers the whole airfield.
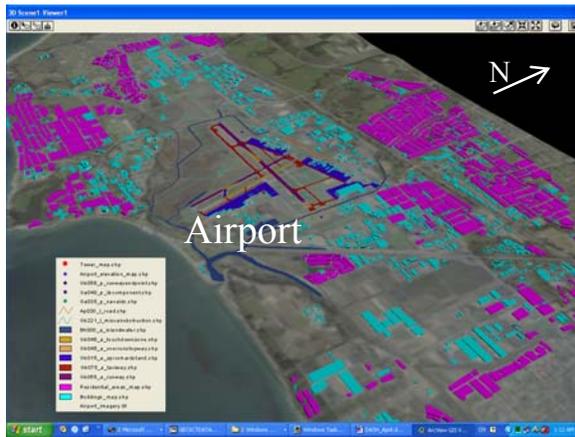
Figure 1. Study area – Santa Barbara Airport

3. METHODOLOGY

3.1 Overview

The first step of the project is to identify airfield obstructions by extracting physical features from Lidar and complying with NIMA's Airfield specification. As airborne Lidar systems have the capability on acquiring digital surface models (DSMs) with high accuracy, and transforming the datasets (scattered 3D points) into grid-base range, the digital terrain models (DTMs) can be generated by using Lidar Expert, which is a toolkit for automated information extraction from lidar data (Hu and Tao, 2004a). Then, the digital non-terrain model (DNM) is produced by subtracting the DTM from the lidar DSM (Hu and Tao, 2004b), and represents all these non-terrain objects including vegetation, buildings and other man-made object, upon a flat reference plane.

Since last-return lidar data is not provided, it is impossible to reliably distinguish buildings from forested areas solely using shape measures. So the potential obstructions are digitized in 2-D manually, and then Lidar Expert is used to extract their heights from raw lidar data. After removing all the digitized man-made objects from the DNM, we get the vegetation height model (VHM), which is the representation of the remaining objects such as trees and bushes.

Next all OIS surfaces are created according to NIMA Airfield Initiative Document. As mentioned before, objects that protrude the OIS or the highest one within one surface regard as obstructions. In order to find all potential obstructions, one of GIS spatial tools, the index model (Lo and Yeung, 2002), is used to generate an obstruction map with three indication levels. The highest one means all obstructions in this level must be removed immediately for the purpose of protecting the National Aviation Infrastructure. The medium means trees, buildings, or other physical objects maybe potential obstructions and need observe periodically. The low means all objects in this level are safe to the airfield. Inside the index model, four OIS-related factors are used: distance to the center line of each runway and its extent, location of objects related to the OIS, type of objects, and penetration related to the OIS. The weights of factors are determined by Saaty Methods. After reclassifying and calculation, the final obstruction map is generated.

3.2 Workflow

In Figure 2, a cartographic model (Michael, 2000) illustrates the workflow of the project. The first part is lidar data processing. It uses filters to generate the DSM, applies image processing and interpolation algorithms to generate the DTM and the DNM. The second part is to digitize buildings and residential areas manually on the aerial DOQ. The forested areas are obtained by subtracting buildings and residential areas from the DNM. The third part is to create seven OIS surfaces, and to digitize bridges, rivers, and roads inside the SVTW. The fourth part is to do geometric correction and bilinear interpolation for scanned topographical map. The new map is used as airfield background. The fifth part is to merge all the features together. Objects extending the OIS should be recorded as airfield obstructions. To help airport managers make a priority decision for obstructions, four new attributes are added. After doing spatial analyses, deriving weights, the finally classified obstructions are identified by raster calculation and are visualized in 3D.

3.3 Data Processing

3.3.1 **Generation of the DTM and DNM:** The direct products of Lidar scanning are DSMs that are formed by the point clouds returned from the top of the Earth's surface partly covered by manmade or natural ground objects. At beginning, the raw Lidar point clouds are filtered to discard outliers or blunders, which have too low or too high elevation values or very large intensity values that do not match their surroundings. A median filter is adopted in this step, because it is useful for removing noise from the original image, especially shot noise by which individual pixel are corrupted or missing. It selects the central value from the lowest to the highest (Jensen, 1996).

The final DTM is derived by applying a hierarchical terrain recovery algorithm (Hu and Tao, 2004). The algorithm identifies terrain points by finding local minima and other topographic points, and recovers the terrain surface in a coarse-to-fine manner. First, after screening the blunders, the scattered 3-D points are transformed into a grid-based range image by selecting the point of lowest elevation in each grid. Then, an image pyramid is generated. The top-level image is hypothesized to be a coarse DTM if its grid size is larger than

the largest non-terrain object. Finally, the coarse DTM is refined hierarchically from the top level to the bottom level. At each level, denser terrain points are identified, and a smooth condition is employed to improve the processing efficiency by integrating information about terrain relief, slope and data density. The non-terrain points are replaced by interpolated elevations using surrounding terrain points. The bottom-level image represents the expected bare Earth surface.
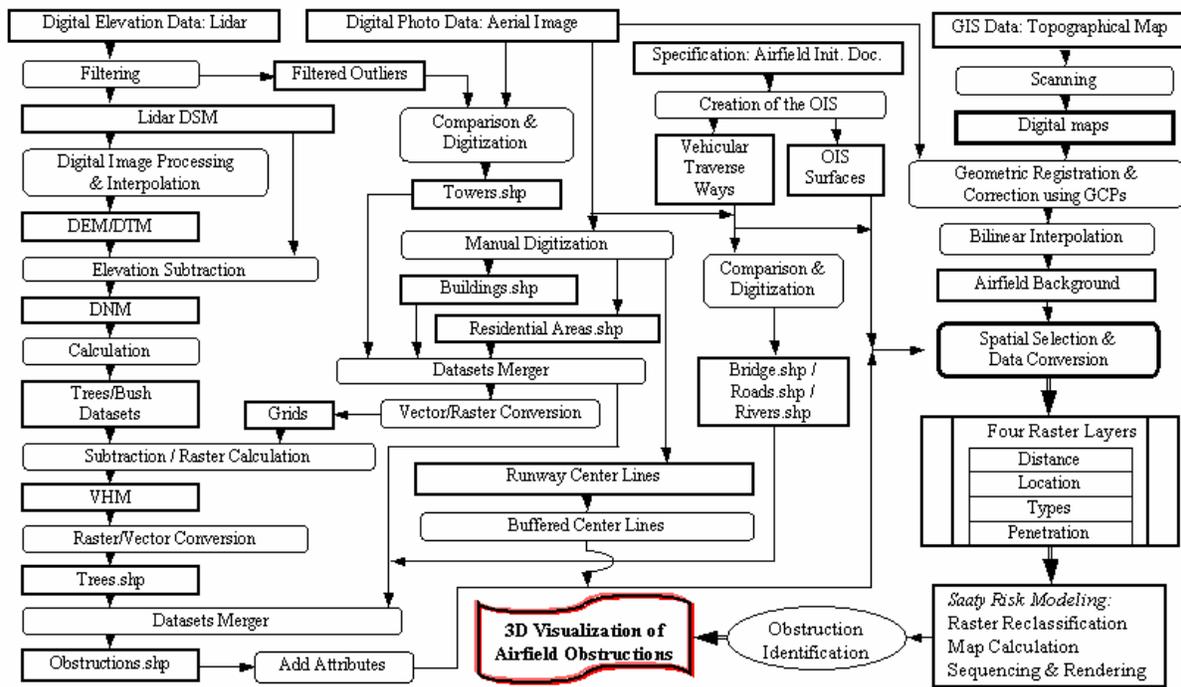
Figure 2. Project workflow

In Figure 3, TIN is used to visualize the continuous surfaces of the DSM (3a) and DTM (3b) (Burrough and McDonnell, 1998).
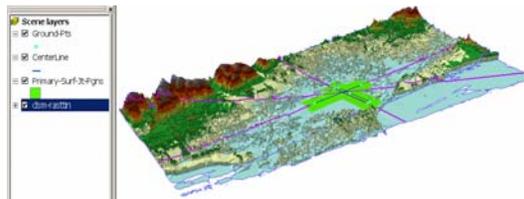
Figure 3a. 3D Visualization of the DSM
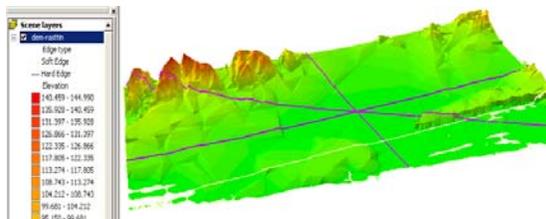
Figure 3b. 3D Visualization of the DTM

Figure 4 shows the two profiles along with the pink diagonal lines in Figures 3a and 3b, respectively. It can be observed that the DSM surfaces are more complex than the DTM's. This is because the DSM includes all non-terrain objects, but the DTM shows the bare terrain surface only.

When the DTM is generated, we also obtain an estimate to the DNM by subtracting the DTM from the raw lidar range image.
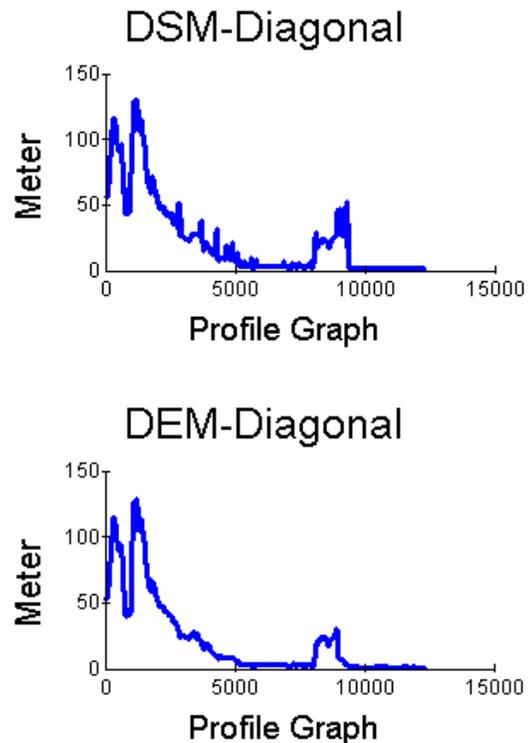
Figure 4. Profiles in the DSM (top) and the DTM (bottom)

The DNM gives a representation of height information of non-terrain objects, including high vegetation, buildings and other objects, relative to the bare Earth surface. The DNM represents all these aboveground objects upon a flat reference plane. Figure 5 shows a profile in the DNM along the same diagonal line as shown in Figure 4.
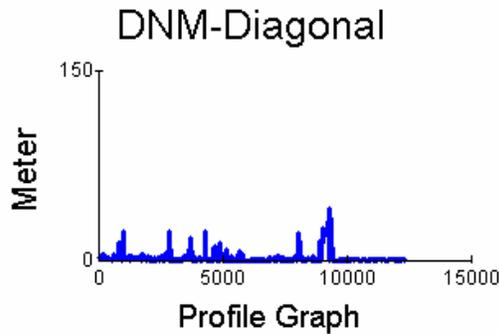
Figure 5. Profile diagonal of DNM

3.3.2 **Digitization of Building Footprints:** Without the bi-return range data, it is impossible to reliably separate the vegetation and buildings in the DNM automatically. Therefore, Those buildings within the IHS are digitized manually on the DOQ. There are total 1,120 building footprints created, and 533 larger polygons representing residential areas. In residential areas, one polygon covers several houses because the heights of houses do not change rapidly. According to NIMA's specification, from DNM, the highest point inside the building footprint is chosen as the roof top. Figure 6 shows all digitized buildings and residential areas exaggerated by 5 times.

Figure 6. Digitized buildings and residential areas

3.3.3 **VHM Generation:** The VHM is created by deleting all the buildings and residential areas from the DNM. First, the layers of buildings and residential areas are converted from features in vector format to grids, and are then deleted from the DNM. The VHM is composed of those grid cells with heights larger than 0.3 m.

3.3.4 **Recovery of Valuable High Points:** Outliers are measured sample points that have very high or very low values relative to the values in a dataset. In the first step of DTM generation, most of removed outliers are correct, such as points reflected by birds, but some valuable points are actually false alarms incorrectly removed. By comparing the photo image with the output of first filtered data carefully, two important towers are found: one is the FAA control tower and another is the general tower. The recovery of these two towers is to get

Z-value from raw lidar data by using the elevation of the highest point within a 100-m diameter circle centering in the footprint of towers. Figure 7 shows the two recovered towers.
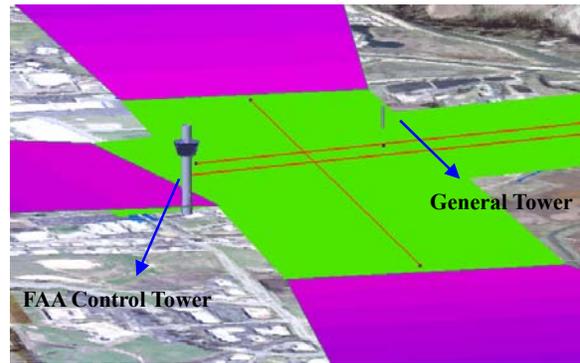
Figure 7. Recovered towers from filtered data

3.3.5 **Geometric Correction:** As the extent of OIS is much larger than the one of airfield photo image, a topological paper map is scanned and used as background for the full scene of OIS. In order to overlap well, the scanned map needs geometric correction, image to image registration. This means two images of like geometry and of the same geographic area are positioned coincident with respect to one another so that corresponding elements of the same ground area appear in the same place on the registered images (Chen and Lee, 1992). Here, the digital photo image of Santa Barbara Airport is assigned as reference map and its spatial coordinates was input to the scanned map. Five ground control points (GCPs) are being selected to register the scanned map to the rectified base photo image. To obtain an optimum effect, all GCPs are located at road intersections with distinct points, and their RMS error is 0.563 m, this means the two maps matched very well (see Figure 8). The left part is the topographical map, and the right is the aerial image. All major roads are exactly aligned. To get a smoother image without stair-stepped effect and high spatial accuracy, the bilinear interpolation is used to resample the geo-referenced map.

Figure 8. Geometrically corrected image

3.4 Create the Airport Glide Path and OIS Surfaces

According to NIMA Airfield Initiative Document, airport glide paths and seven OIS surfaces are created. Figures 9 & 10 shows these OIS surfaces in 2-D and 3-D, respectively. To avoid airport incursion, the features within the SVTW, including roads, railroads, bridges, rivers and ponds, are also digitized.

Not to Scale
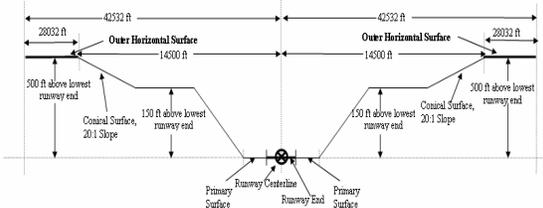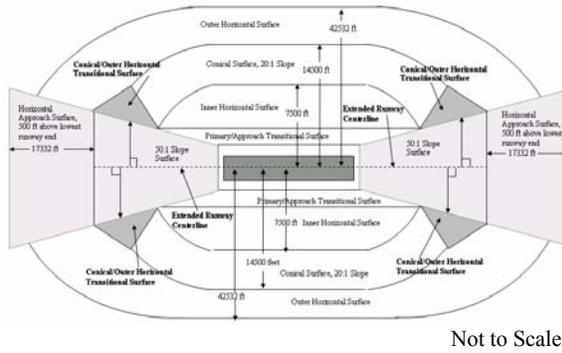
Figure 9. Top View (top) and end view (bottom) of 2D OISs
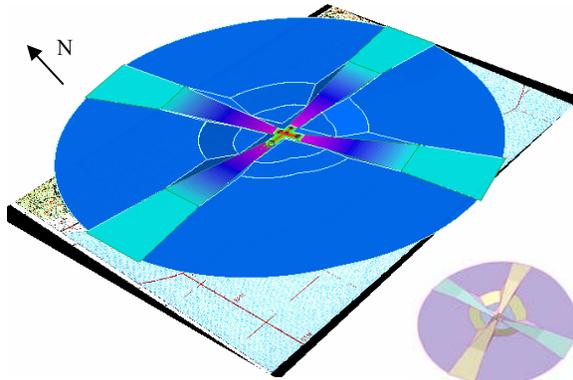
Figure 10a.   3-D OIS with geometrically corrected map
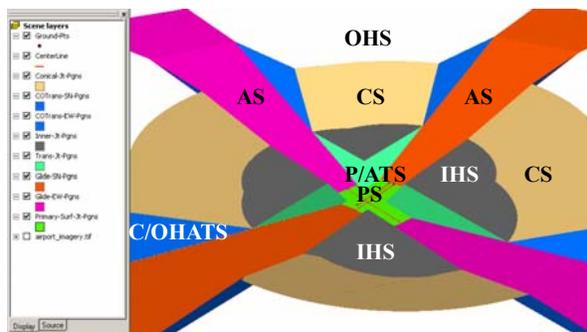
Figure 10b. 3-D View of Draped OIS (Separated Layers)

3.5 Datasets Merger

Table 1 list all the features digitized within the IHS. For the convenience of processing, these features are overlaid and merged together to create a new map. The measured features and extracted data include all the required data for the OIS analysis and their accuracies are better than the accuracy required for obstruction identification.

Features	# of objects
Buildings	1120
Residential Areas	533
Recovered Towers	2
Tree Areas	233
Airfield Features	12
Roads	(7)
Rivers	(2)
Ponds	(1)
Bridges	(2)
SUM	**1890**

Table 1. Digitized airfield objects within HIS

4.   OBSTRUCTION IDENTIFICATION AND RISK-RATING RESULTS

All the digitized airfield objects that protrude the OISs are identified to support a safe flying environment. These identification results can help airport managers to check if their airfields meet the new safety requirements. To provide a clear view of the priorities of airfield obstructions to airport managers, the identified obstructions are classified into three risk categories by assessing risk index scores. A RI is computed for each obstruction as a weighted sum of four risk factors, each corresponding to evidence upon which the risk evaluation is based. A larger RI score implies that the obstruction is more dangerous. The equation reads:

$$RI_{obstruction} = w_1R_1 + w_2R_2 + w_3R_3 + w_4R_4,$$
$$\text{w.r.t.} \qquad w_1+w_2+w_3+w_4=1 \qquad (1)$$

where R_i is the risk score of factor i (1 to 4); w_i is the weight of factor i. The higher the weight, the more influence a particular factor will have in the index model. Each risk factor is assessed a score within the range of 1 to 5 as shown in Table 2.

Risk levels	Low	Median		High	
	1	2	3	4	5
Distance (m)	< 2286	< 1000	< 600	< 300	< 100
Location	OHS, C/OHATS	CS	PS	IHS, P/ATS	AS
Type	Mountains	Residential houses	Objects within SVTW	Trees	Towers, buildings
Protrusion	N/A		OHS, C/OHATS	PS, CS	AS, IHS, P/ATS

Table 2. Risk levels of four risk factors

Four risk factors are evaluated to take into account distance, location, type and protruding condition as described below:

- Distance factor R_1 is measured by the distance of an obstruction from the centerline of a runway. The risk levels are determined by the distance from the HIS layer within 2,286 meters.
- Location factor R_2 is measured by the position of an obstruction related to OIS. Different OIS layers are assigned with different risk levels.
- Type factor R_3 is measured by the obstruction types, including buildings, trees, houses, mountains etc. For example, buildings are more dangerous than trees.
- Protrusion factor R_4 is the measurement of the protruding condition. An obstruction protrudes any OIS has a risk level

of no less than 3.

The weights in Eq. 1 can be approximated by dividing the sum of values at that row by the total sum (i.e., the shaded cell in Table 3). Saaty (1980) determined the weights using the analytic hierarchy process, which makes a series of pair-wise comparisons to determine the relative importance and ensures consistency between all the factors in a multi-criteria evaluation. In Table 3, a pair-wise comparison matrix is constructed, where each factor is compared with the other factor, relative to its importance, on a scale from 1 to 9. The empirical values about the comparative importance between every two factors are shown in Table 3. The weights are obtained by scaling the principal eigenvector of the matrix, that is, (0.13, 0.23, 0.05, 0.59). For example, the mountain summits sited at the northwest corner are about 1700 m from the HIS and protrude the C/OHATS (see Figure 10b). Their risk index is equal to 2.09 as calculated using Eq. 1 with weights substituted.

Risk factors	R_1	R_2	R_3	R_4	Row sum	Weight
R_1	1	1/2	3	1/5	4.70	0.14
R_2	2	1	5	1/3	8.33	0.26
R_3	1/3	1/5	1	1/9	1.65	0.05
R_4	5	3	9	1	18.00	0.55
Sum					32.68	1.00

Table 3. Comparison of the relative importance of factors

Saaty (1980) calculates a consistency ratio (*CR*) to check the probability that the ratings are randomly generated. The CR is defined by Eq. 2, where λ_{max} is the principal eigenvalue of the matrix; *n* is the number of factors. A matrix with the CR value greater than 0.1 should be re-evaluated, and the process is repeated until the CR is less than this threshold. The CR is 0.0123 for the matrix in Table 3.

$$CR = (\lambda_{max} - n) / (n - 1) \qquad (2)$$

A risk level for each obstruction is assessed, and a part of the risk-rating map is shown in Figure 11. The high-risk obstructions pose a severe threat to aircrafts and should be removed to conform to the AID. The median-risk obstructions may be kept, but should be inspected periodically.
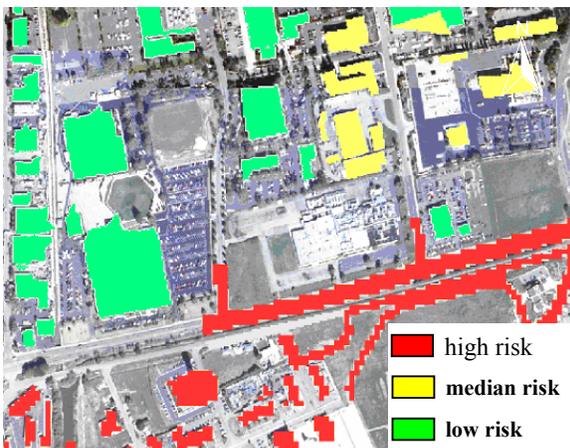
Figure 11. Obstructions risk-rating map

5. CONCLUDING REMARKS

By combining lidar data processing techniques with photogrammetric mapping services, new toolsets help airfield monitors solve problems and make decisions. In this paper, we present an approach for identifying airfield obstructions according to the new safety requirements in the Airfield Initiative Document published by NIMA. The obstructions include all kinds of physical features, and airport manager can directly select all the dangerous obstructions from the risk-rating mapping results. Next, we will setup an automatic model on the OIS creation and object extraction. This will meet the extremely urgent requirements of obstruction identification from 7,200 airports in the US and an undetermined number of airports, worldwide.

6. REFERENCES

Burrough, P., McDonnell, R.A., 1998. *Principles of Geographical Information Systems*. Oxford University Press.

Chen, L., Lee, L., 1992. Progressive Generation of Control Frameworks for Image Registration. *Photogrammetric Engineering & Remote Sensing*, 58(12): 1321-1328.

Hu, Y., Tao, V., 2004a. Lidar Expert: a toolkit for information extraction from airborne lidar data. *Proc. of the ASPRS Annual Conference*, 23-28 May, Denver, 9 p.

Hu, Y., Tao, V., 2004b. Hierarchical recovery of digital terrain models from single and multiple returns lidar data. *Proc. of the ASPRS Annual Conference*, 23-28 May, Denver, 12 p.

Jensen, J.R., 1996. *Introductory Image Processing: A Remote Sensing Perspective*. Prentice Hall, 156 p.

Lo, C.P., Yeung, A.K.W., 2002. *Concepts and Techniques of Geographic Information System*. Prentice Hall, 152 p.

Michael N.D., 2000. *Fundamentals of Geographic Information Systems* (2nd Edition). John Wiley & Sons, Inc.

Morain, S.A., 2001. Remote Sensing for Transportation Safety, Hazards, and Disaster Assessment. *Urban Geoinformatics*, 16-19 October, Wuhan, 6 p.

National Imagery Mapping Agency (NIMA), 2001. *Airfield Initiative Document*, 50 p. URL: http://www2.nima.mil/products/rbai/AIDOCwww.zip.

Saaty, T.L., 1980. *The Analytical Hierarchy Process: Planning, Priority Setting, Resource Allocation*. McGraw-Hill International Book Co., New York, 287 p.

TRB, 2002. Airfield inactive remote sensing technologies evaluation project. *Remote Sensing Conference*, December 2002, 8 p.